Electronic Supplementary Material (ESI) for ChemComm.

Supporting Information

Lattice-Strained Palladium Nanoparticles as Active Catalyst for Oxygen Reduction Reaction

Jing-Yang Lin, Cong Xi, Zhe Li, Yi Feng, De-Yao Wu, Cun-Ku Dong, Pei Yao, Hui Liu, Xi-Wen Du*

Institute of New-Energy Materials, School of Materials Science and Engineering, Tianjin University, Tianjin 300350, China.

Correspondence to: xwdu@tju.edu.cn

This file includes:

Methods

Supporting Figures S1-S9

Supporting Table S1-S2

1. Methods

Synthesis of L-Pd NPs. L-Pd NPs were produced by laser ablation of a palladium target immersed in an aqueous solution of NaCl. Nd:YAG laser (Dawa-350, Beamtech) was operated at wavelength 1064 nm, pulse width 7 ns, single-pulse energy 200 mJ, frequency 15 Hz. Specifically, a piece of Pd tablet (30mm*30mm*1mm, 99.99%) was first abrasive by sandpaper to remove the surface oxide layer, followed by rinsing with deionized water. Next, the Pd target was immersed in a 0.01 M aqueous solution of NaCl with its upper surface ~20 mm lower than the solution level, and then ablated by the pulsed laser for 10 min at room temperature. The as-obtained suspension mixed with carbon black at a Pd/C mass ratio of 1:4. The mixture was firstly ultrasonically treated and then centrifuged. The precipitate was rinsed with deionized water for five times, and subsequently dried in vacuum to get the final product.

Synthesis of A-Pd NPs. L-Pd NPs were loaded on SiO_2 microspheres and annealed in N_2 at 300 ℃ for 2 h. The annealed product was dissolved in 5 M KOH, and then stirred for 30 min to remove SiO_2. After that, the solution was centrifuged washed with deionized water for five times, and finally dried in vacuum.

Characterizations. TEM images were acquired by using an FEI Tecnai G2 F20 transmission electron microscope. X-ray diffraction patterns (XRD) were taken on a Bruker D8 Advance diffractometer. STEM-HAADF images were obtained by JEOL ARM-200F equipped with a cold field emission gun and a Cs corrector (CEOS) for probing lenses at the operation voltage of 200 kV. XAS measurements were carried out at experimental station of the Stanford Synchrotron Radiation Light Source.

Electrochemical measurements. 5 mg of the as-prepared catalyst were ultrasonically dispersed in 1 mL od DI water, followed by the addition of 15 μL of Nafion solution (5 wt%) into the solution. The mixture was ultrasonicated to obtain a homogenous catalyst ink. Proper amounts of the electrocatalyst ink were then transferred onto glassy carbon rotating disk electrode (RDE, 0.196 cm^2) or rotating ring disk electrode (RRDE, 0.247 cm^2) to keep a constant catalyst mass loading of 0.4 $mg \cdot cm^{-2}$ for all the measurements. The electrodes were then dried in air and served as a working electrode.

Electrochemical measurements of samples were carried out in a three-electrode electrochemical cell configuration including a graphite counter electrode, a saturated calomel reference electrode, and a working electrode. The reference electrode was calibrated in H_2-saturated 0.5 M H_2SO_4 solution before measurements. For ORR, four catalysts were adopted as the working electrode, whose performance was measured in O_2-saturated 0.5 M H_2SO_4 aqueous solution. All experiments were carried out at 25 ℃. Before data collection, cyclic voltammetry (CV) curves were repeatedly recorded at scan rate of 50 $mV \cdot s^{-1}$, until the signals were stabilized. Then linear sweep voltammograms (LSV) were measured at a scan rate of 5 $mV \cdot s^{-1}$.

The transferred electron number and the corresponding H_2O_2 formation on electrodes during the ORR process was derived from the RRDE data by the following equations:

$$\%H_2O_2 = \frac{200i_r/N}{i_d + i_r/N}$$

$$n = \frac{4i_d}{i_d + i_r/N}$$

where N is the collection efficiency of the RRDE (0.37), and i_d and i_r are the disk and ring electrode currents, respectively.

RDE voltammograms of ORR on L-Pd catalyst were received at different rotation rates from 900 rpm to 2500 rpm at a scan rate of 5 $mV \cdot s^{-1}$ (see Fig. S6). The RDE data was analyzed using KouteckyeLevich (K-L) equations:

$$\frac{1}{j} = \frac{1}{j_k} + \frac{1}{j_d} = \frac{1}{nFkC_{O_2}} + \frac{1}{B\omega^{1/2}}$$

$$B = 0.2nFC_{O_2}D_{O_2}^{2/3}\nu^{-1/6}$$

where J, J_d, and J_k represent the measured current density, diffusion-limiting current density, and kinetic current density ($mA \cdot cm^{-2}$), respectively; n is the electron transfer

number per O_2; A is the surface area of working electrode (0.196 cm^2); F and T are the Faraday constant (96485.3 $C \cdot mol^{-1}$) and temperature, respectively; D_{O_2} and C_{O_2} are the oxygen diffusion coefficient (1.9×10^{-5} $cm^2 \cdot s^{-1}$) and the bulk concentration (1.2 $mM \cdot L^{-1}$), respectively; ω is the rotation rate of electrode ($\omega = 2\pi \times$ rpm, $rad \cdot s^{-1}$); k is the electron-transfer rate constant.

Computational method. The plane-wave based density functional theory (DFT) method with the Vienna Ab Initio Simulation Package (VASP)[1-3] were applyed on Pd (111) facet to uncover the cause of ORR performance improvement. The Perdew-Burke-Ernzerhof (PBE) functional within the generalized-gradient approximation (GGA) range was employed for exchange-correlation function[4]. An energy cut-off of 500 eV was used to ensure accurate energies. Geometry optimization was completed when all forces became smaller than 0.03 $eV \cdot Å^{-1}$. The vacuum layer of 15 Å between periodically repeated slabs was set to avoid interactions among slabs. The K-point for all structures was set to be 3×3×1 in this study. Pd is a face centered cubic structure with a lattice constant of 3.8907 Å and the compressive strain was applied on the cubic by reducing 3% of lattice length in three dimensional before Pd (111) surface was cleaved. The computational structures were four layers tall with a three atoms by three atoms surface area. During calculation, the bottom two layers of structures were fixed while the top two layers of them were allowed to relax to ensure a full interaction between metal atoms and adsorbate atoms.

The adsorption energy (E_X^{ads}) of each intermediate (X) was calculated by the following equation,

$$E_X^{ads} = E_{*X} - E_* - E_X$$

where E_{*X}, E_* and E_X are energies of Pd (111) surface with intermediate, clean Pd (111) surface, and each intermediate.

The Gibbs free energy (G) of the adsorbed intermediate on the DFT scale was calculated by

$$G = E_{DFT} + ZPE - TS$$

where E_{DFT} is the total electronic energy obtained with DFT, *ZPE* is the zero-point-energy correction and S is the entropy of the system obtained through vibrational-frequency analysis using the harmonic oscillator approximation.

Supporting Figures

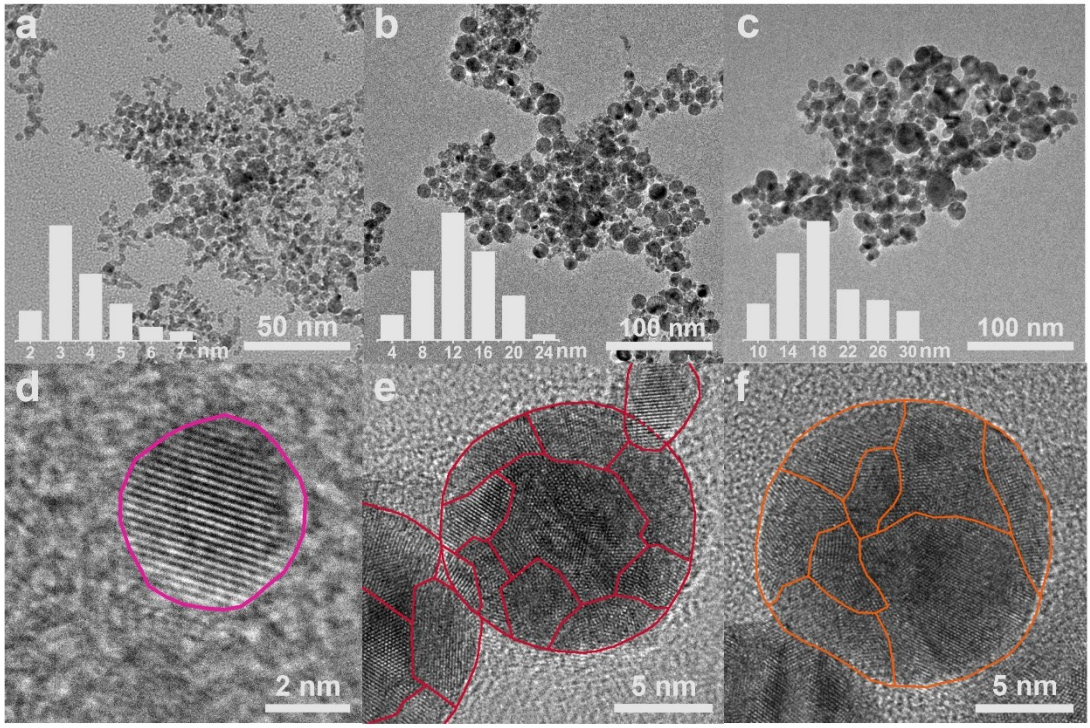

Fig. S1 The influence of NaCl concentration on the morphology and structure of L-Pd NPs. (a), (b), (c) are TEM images of the products obtained in 0.1, 0.01 and 0.001 M NaCl solution, respectively. (d), (e), and (h) are HRTEM images of the products obtained in 0.1, 0.01 and 0.001 M NaCl solution, respectively. The grain boundaries are highlighted with colorful lines.

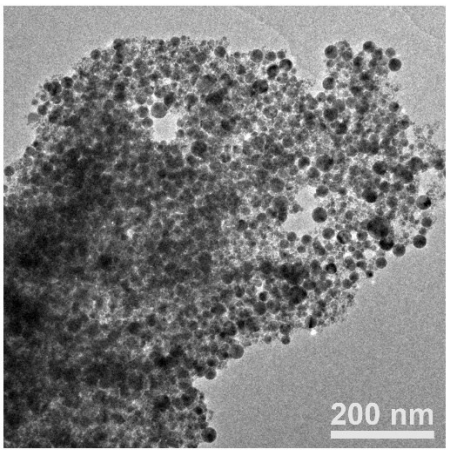

Fig. S2 TEM image of Pd NPs synthesized by PLAL in pure water without NaCl.

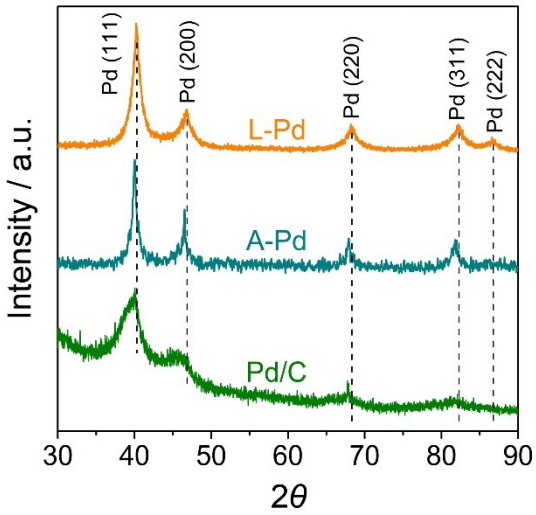

Fig. S3 XRD patterns for L-Pd, A-Pd and Pd/C.

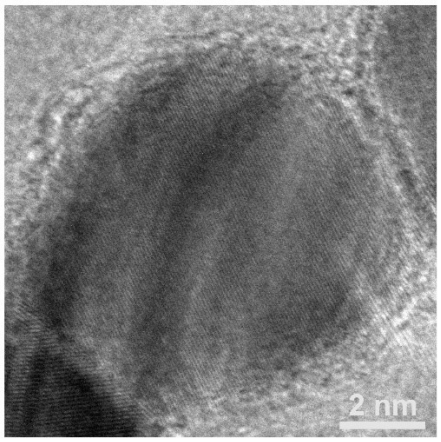

Fig. S4 HRTEM image of an A-Pd nanoparticle.

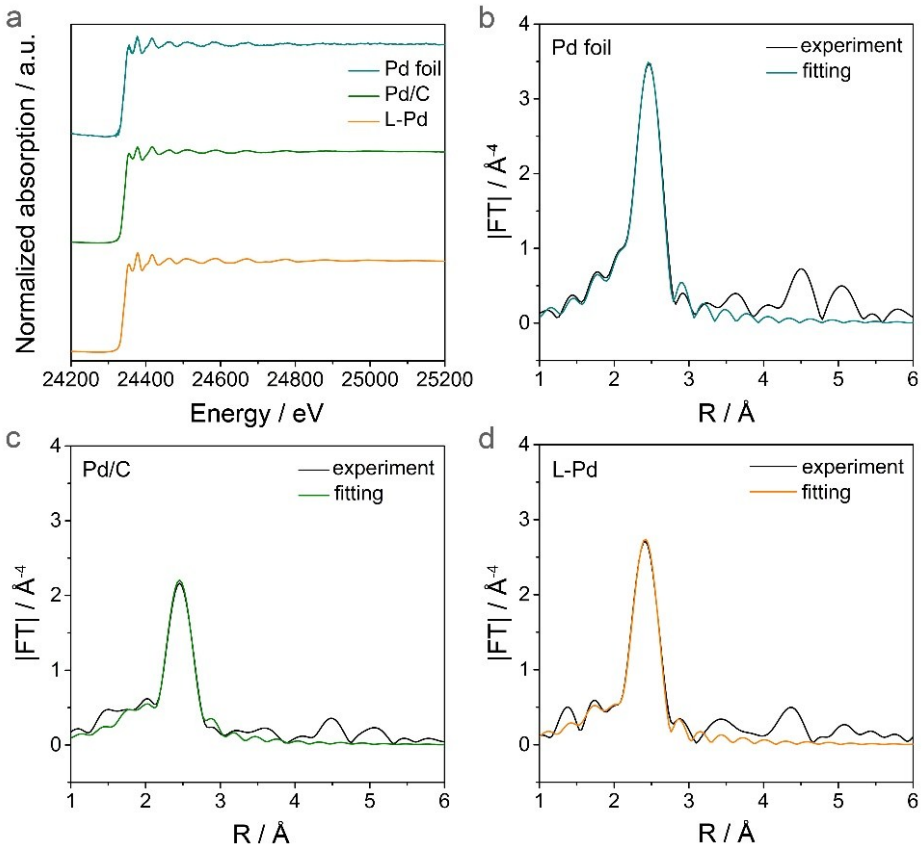

Fig. S5 XAS analysis on Pd foil, Pd/C and L-Pd. (a) XAFS spectra; (b), (c) and (d) are experimental and theoretical fittings of FT EXAFS spectra of Pd foil, Pd/C and L-Pd, respectively.

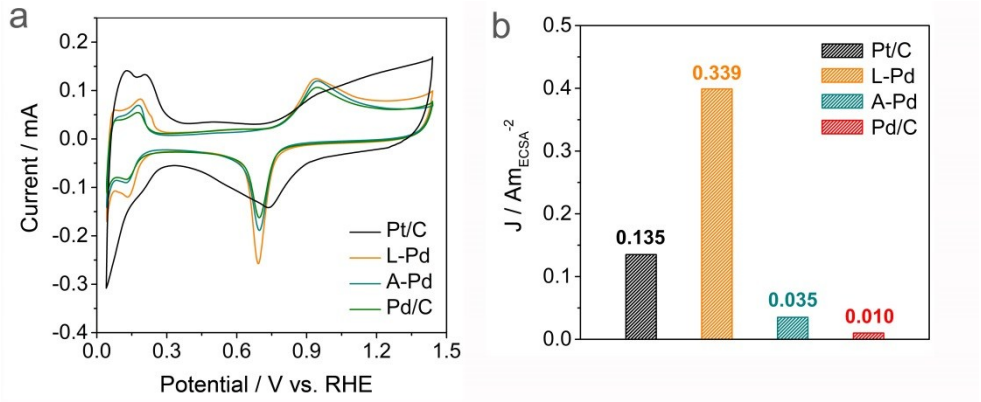

Fig. S6. Calculation on specific activities of Pt/C, L-Pd, A-Pd and Pd/C in 0.5 M H_2SO_4 solution. (a) Typical cyclic voltammetry curves for calculating ECSA values which are determined as 71.59 $m^2 \cdot g^{-1}$ for Pt/C, 22.78 $m^2 \cdot g^{-1}$ for L-Pd, 21.85 $m^2 \cdot g^{-1}$ for A-Pd, and 18.31 $m^2 \cdot g^{-1}$ for Pd/C). (b) SA values calculated at the half-wave potential (0.78 V vs. RHE)

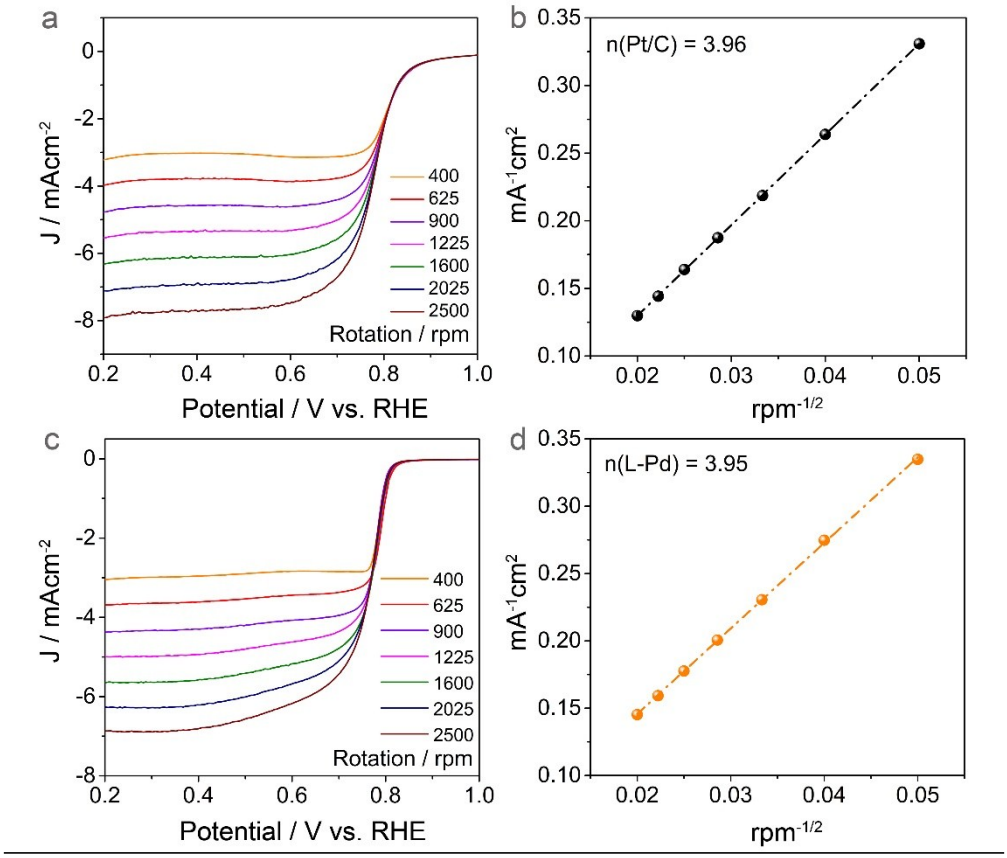

Fig. S7 RDE measurements of (a) Pt/C and (c) L-Pd at rotation rates from 900 to 2500 rpm and a scan rate of 5 $mV \cdot s^{-1}$. (b) and (d) are corresponding K-L plots of Pt/C and L-Pd, respectively.

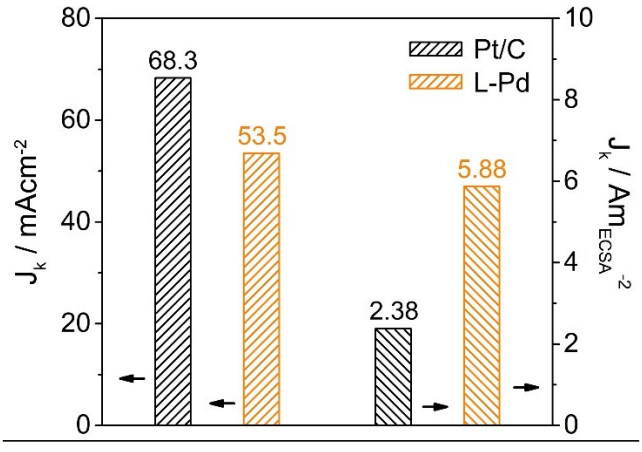

Fig. S8 Kinetics currents of L-Pd and Pt/C before and after normalized by ECSA

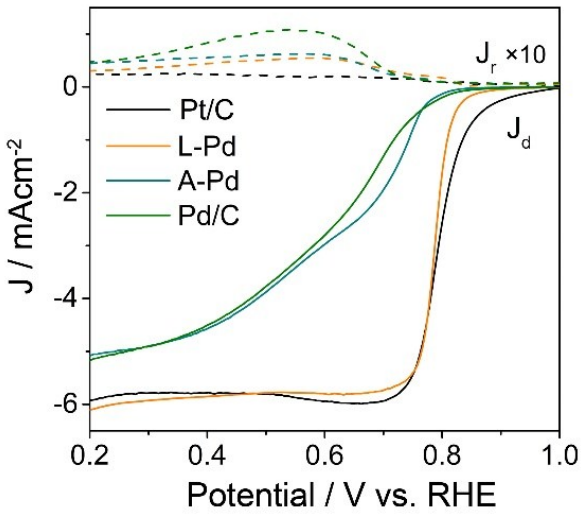

Fig. S9. The RRDE measurements of L-Pd, A-Pd, Pt/C and Pd/C samples.

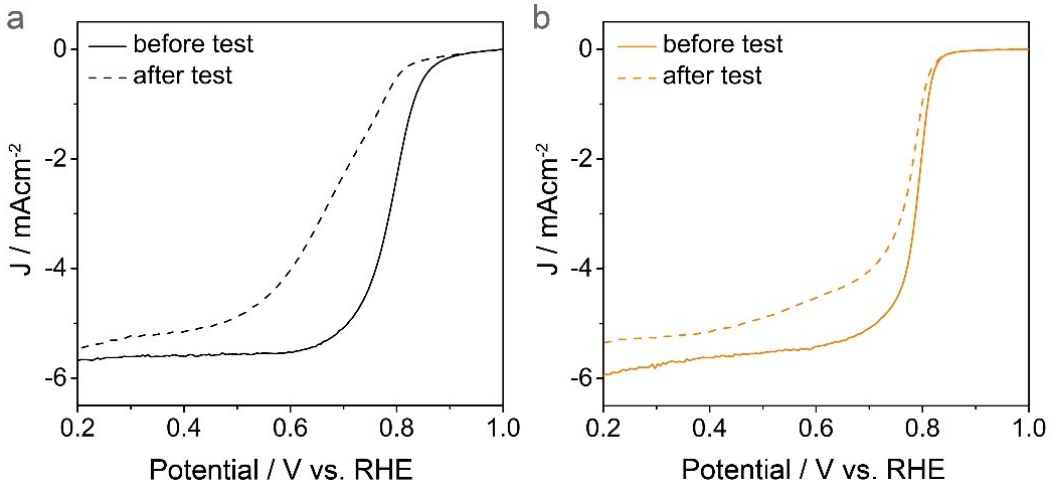

Fig. S10. LSV curves before and after ORR stability test of (a) L-Pd and (b) Pt/C.

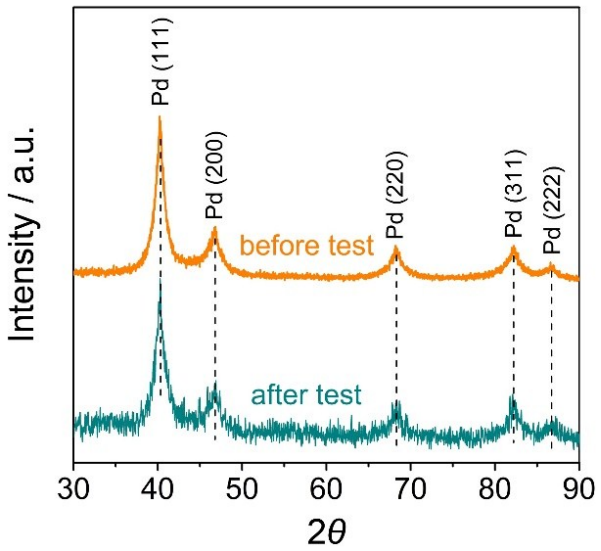

Fig. S11. XRD patterns for L-Pd before and after ORR stability test.

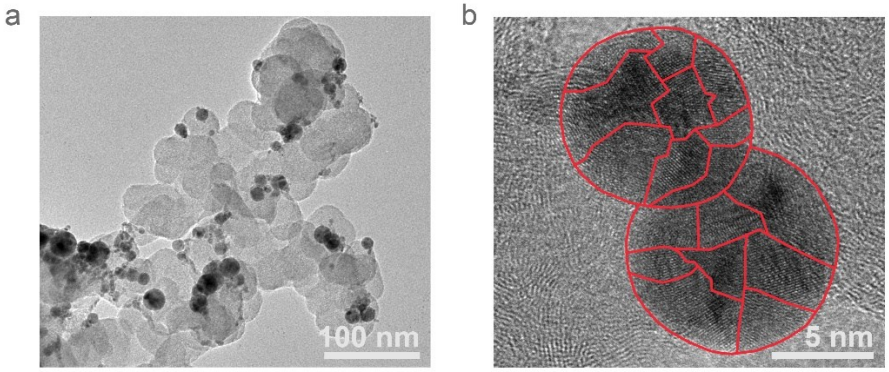

Fig. S12. TEM images of L-Pd after ORR stability testing for 10 h. (a) Low magnification TEM image. (b) HRTEM image.

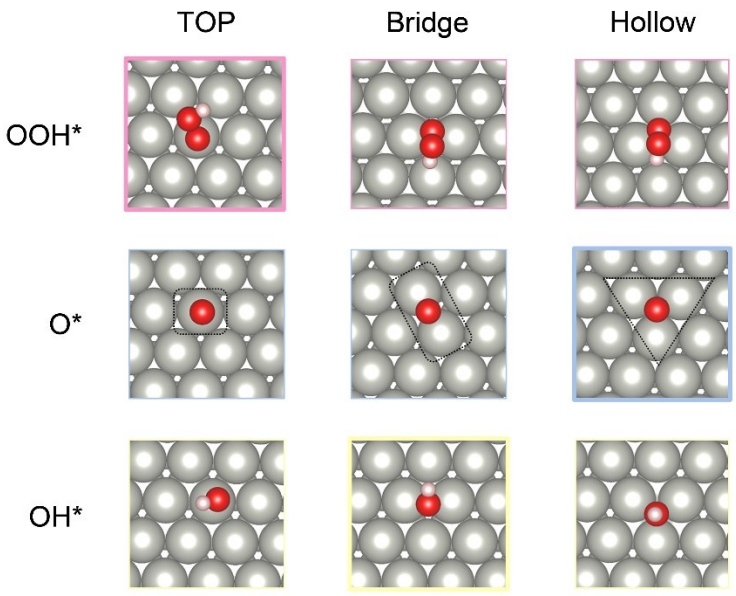

Fig. S13. Top, bridge and hollow adsorption sites for OOH*, O* and OH* in computational models. Top, bridge and hollow sites are the positions where absorbing atoms stay right on one Pd atom, in the middle of two Pd atoms and in the center of three Pd atoms in (111) facet, respectively, as indicated in the frame for O*. The stable adsorption structures are highlighted with bold borders.

Supporting Tables

Table S1. Relative adsorption energies (eV) of intermediates for structures without strain (left side with black font) and with strain (right side with red font). The values for the most stable sites are shown in bold.

Species / Sites	OOH*	O*	OH*	OOH*	O*	OH*
Top	**0.00**	1.38	0.17	**0.00**	1.30	0.13
Bridge	0.10	unavailable	**0.00**	0.001	0.004	**0.00**
Hollow	0.11	**0.00**	0.11	unavailable	**0.00**	0.20

Table S2. The zero-point-energy correction (*ZPE*), entropy (*S*) and Gibbs free energy difference (*ΔG*) of intermediates for both origin (left values with black font) and strain (right values with red font) structures.

	OOH*	O*	OH*	*	OOH*	O*	OH*	*
ZPE	0.22	0.03	0.23	--	0.22	0.03	0.23	--
TS	0.24	0.04	0.10	--	0.24	0.04	0.09	--
ΔG	-1.76	-2.18	-0.43	-0.54	-1.72	-2.12	-0.45	-0.62

References

1. J. F. l. G. Kresse, *Physical Review B*, 1996, **54**, 11169-11186.
2. G. Kresse and J. Hafner, *Physical Review B*, 1993, **47**, 558-561.
3. G. Kresse and J. Hafner, *Physical Review B*, 1994, **49**, 14251-14269.
4. K. B. John P. Perdew, Matthias Ernzerhof, *Physical Review Letters*, 1996, **77**, 3865-3868.